BRIEF COMMUNICATION   **OPEN**

Check for updates

Faint yet widespread glories reflect microphysics of marine clouds

Ilan Koren [1,4✉], Alex Kostinski [2,4], Uri Wollner[1] and Daria Dubrovin[1,3]

Glory is a beautiful optical phenomenon observed in an atmosphere as concentric colored rings reflected by clouds or fog around an antisolar point. Here we report that true color glories, although faint, are discernible in raw unpolarized satellite images by a naked eye on a daily basis, thus constituting a large and untapped reservoir of cloud data for which a simple diffraction-like approximation links cloud droplet diameter and variance to the glory's structure.

Marine stratocumulus (Sc) clouds cover much of the eastern parts of subtropical oceans and form ~1000 km-long decks of shallow but highly reflective clouds[1]. These Sc clouds turn the mostly black ocean (low albedo) into a giant reflector that scatters much of the incoming solar radiation back to space, and therefore acts as an important cooling component of the climate system. Earth albedo is sensitive to Sc microphysics because cloud droplet sizes are comparable to the range of wavelengths of incoming solar and outgoing infrared radiation. Moreover, the droplet size distribution is entangled with other clouds properties such as precipitation and lifetime. Therefore, size distribution of droplets is an important property to retrieve[2,3].

As other colorful atmospheric phenomena, optical glory features decomposition of incoming white sunlight into distinct wavelengths. Such processes tend to involve limited interaction of solar radiation with clouds or rain drops, e.g., single backscattering in the case of glory. Therefore, the information on glory arrives from within approximately one mean free path of photons and samples mostly the upper part of the cloud. Unlike rainbows and haloes, glory still lacks a simple physical explanation[4].

About twenty years ago it was observed from space[5] for the first time and has, since then, occasionally provided spectacular shots in satellite images. The glory has a streaked geometry and requires perfect sun-satellite-cloud alignment. The elongation of the glory along the orbital track results from real time image processing by the satellite. Only the transverse dimension is needed to infer cloud droplet size and along-track sampling then permits an estimate of a larger portion of the Sc deck. The estimated tens of thousands of such glories in MODIS images alone constitute an untapped reservoir of cloud microphysics information. This is complementary to the existing radiative transfer based methods because droplets sizes are retrieved here from well-characterized cloud tops and optically thin clouds. Moreover, the glory properties are sensitive to both first and second moments of the cloud's droplet size distribution (DSD), i.e., the mean radius and the variance[6,7]. Retrieving such pairs yields insights into cloud's properties.

Traditionally, droplets sizes are retrieved from space parametrically by assuming multiple scattering, employing relations between scattering and absorbing wavelengths, and inverting for the cloud optical thickness and effective radius simultaneously,

e.g., Nakajima-King (NK) method[8]. However, these methods, while generally reliable and well tested, fall short of retrieval from optically thin clouds (cloud optical depth, $\tau < 1$) and/or small droplets as in the case of some marine Sc droplets. Furthermore, such methods are insensitive to the DSD variance. To that end, Fig. 1 shows that faint yet ubiquitous glories, readily found on a daily basis in satellite data (Fig. 2), supplement conventional retrievals by supplying top of the cloud droplet size information for Sc clouds and bypassing optical depth. Moreover, such variables as temperature, pressure, and height are measured best at cloud tops and knowing the droplet size there is particularly useful.

For glory, optically thin clouds and small droplets is the optimal combination that yields information, complimentary to the traditional methods. Then one has two samples of the droplet radius vertical profile rather than a single one because the droplet size information from, say, NK retrievals comes from deeper parts of the cloud as multiple scattering arises from all parts of the cloud and the effective radius changes with the shape of the size distribution.

Figure 1a depicts the method which is then applied to the data of Fig. 2, for May 29, 2021, MODIS-Aqua satellite image of a cloud deck over the Pacific, off the coast of Baja California. The upper (northern) half of the faint glory is seen over thicker clouds with τ in the visible $\sim O(10)$, in contrast to the lower half with $\tau \sim O(1)$. Readers may note the broadening of the glory over the shallow cloud portion, (in agreement with the simple diffraction scaling $\Delta\theta \sim d^{-1}$) and the tendency of droplet sizes to correlate with cloud thickness.

The ratio D/H, as shown in Fig. 1a, links to the glory's angular size $\Delta\theta$, the latter inversely proportional to the droplet's diameter d. For the Fig. 2b segment, the Aqua satellite elevation of 705 km and the distance between the satellite to the center of the glory is $H = 757\pm1$ km as the glory's center angle from nadir (marked in Fig. 1-a) is $\alpha = 21.4 \pm 0.1°$. Eyeballing the spatial extend of the red ring straight from the faint image Fig. 2.a is imprecise but the processed Fig. 2b (magenta box) yields $D \approx 61$ km ± 1 km and $\Delta\theta = 61/757 \approx 0.08$ rad.

The continuously reported data on the satellite zenith angle yields an equally simple but a more direct and accurate measure for $\Delta\theta$ (see Methods). As shown in Fig. 2c, the glory's angular size and the related magnitudes are readily obtained from the measured

[1]Department of Earth and Planetary Sciences, Weizmann, Institute of Sciences, 234 Herzl St., Rehovot 7610001, Israel. [2]Department of Physics, Michigan Technological University, 1400 Townsend Dr., Houghton 49931 MI, USA. [3]HEMDA, the Schwartz-Reisman science education center, 7 Hapardes St., Tel Aviv Yafo 610101, Israel. [4]These authors contributed equally: Ilan Koren, Alex Kostinski. ✉email: ilan.koren@weizmann.ac.il
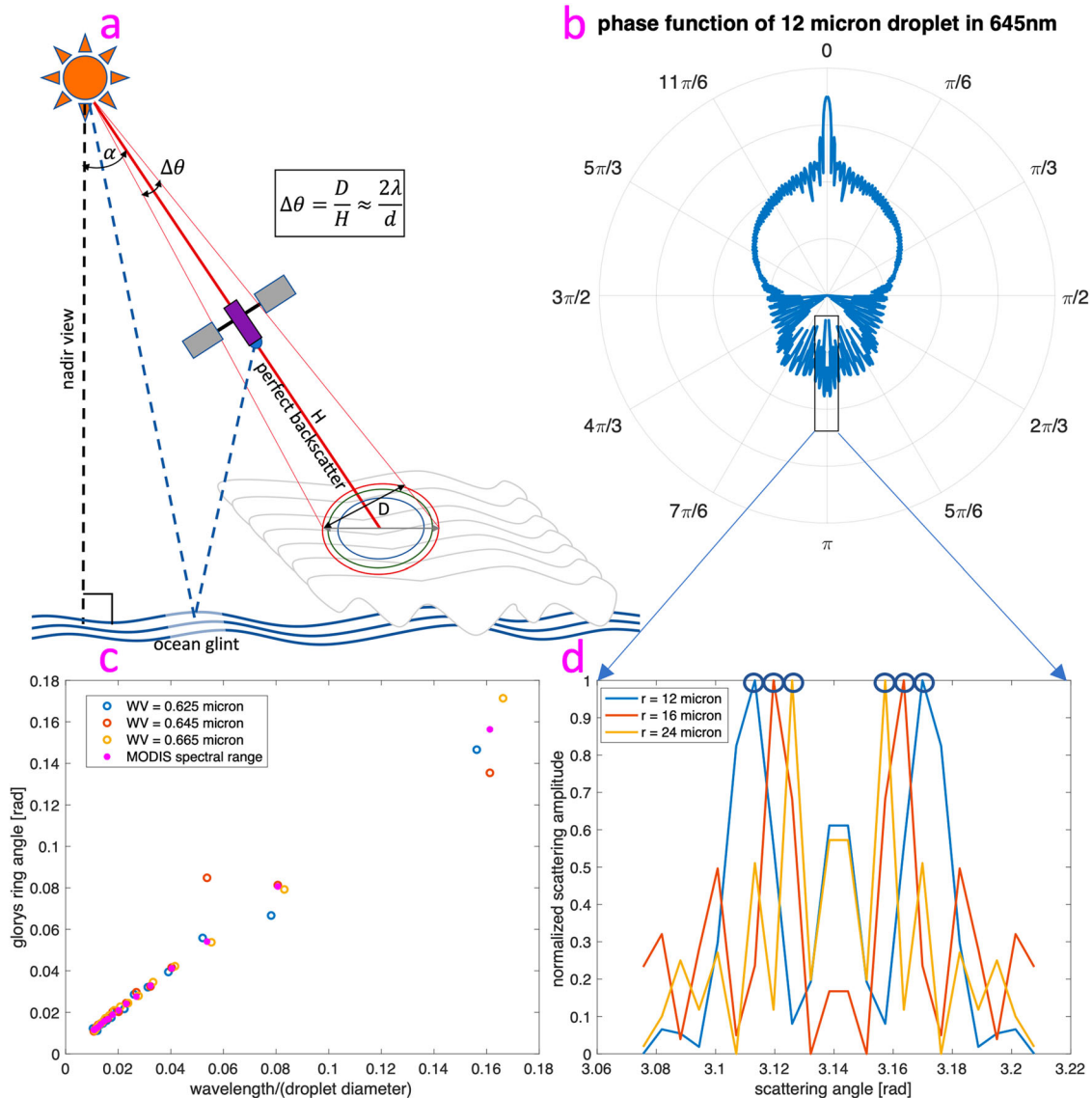
Fig. 1 How optical glory yields a cloud droplet diameter. a Glory's geometry—The glory angular size, $\Delta\theta \equiv D/H$, with H denoting the distance between the glory's center and the satellite and D, the diameter of the inner (red) ring in the satellite image, projected onto the normal to H, is approximately equal to $2\lambda/d$ with d being the droplet size and λ, the wavelength of (red) light. **b** Polar diagram of the scattered light logarithmic intensity vs. the scattering angle. Because of the large optical size of cloud droplets, most of the incident radiation is scattered forward and the entire diagram is not only complex, with intricate details but also highly sensitive to small changes in wavelength, particle size, and index of refraction. A mere 20 nm change in the droplets radius, a relative change of 0.2%, yields doubling of the glory peak amplitude. Yet, despite such sensitivity, **c**, based on the exact solution for scattering by a water sphere, shows that a simple diffraction-like scaling suffices to link the angular size of the glory to the scaled inverse droplet diameter, λ/d. **d** Closeup of the phase function near perfect backscatter (glory) as demarcated by the black rectangle of **b**. Changes in the width of the glory ring are shown for three droplet radii.

reflectance of the red channel along the middle part of the glory's ring (magenta box in Fig. 2b). The glory's angular size $\Delta\theta = 0.0803 \pm 0.0024$ rad $= 4.6 \pm 0.14°$ as indicated by arrows in Fig. 2c. Based on theoretical Mie calculations such as the ones shown in Fig. 1c, the pre-factor for the MODIS red (645 nm) range is $\eta = 1.98$. Therefore the retrieved droplet diameter is $d = \eta \times \lambda_{red}\left(\frac{H}{D}\right) = \eta \times \lambda_{red}/\Delta\theta = 1.98 \times 0.645/0.0803 = 15.9 \pm 0.5\mu m$

This "back-of-the-envelope" value of d is calculated for the glory of a monodisperse cloud droplet population. The actual value of the mean diameter d is somewhat smaller because larger droplets contribute more to the superposition of glories. The true value of mean d and the DSD variance can be retrieved simultaneously by using the information on $\Delta\theta$ and on the Bessel-like modulation of the spatial pattern, that is the amplitude ratio of the perfect back-scatter to the first glory ring (see Methods). The measured pairs in

this case yielded ($r = 6.9\,\mu m, \sigma = 1.75\,\mu m$) for the left half and ($r = 6.6\,\mu m$, $\sigma = 2.21\,\mu m$) for the right half of the glory. These values of about 13 microns for the mean droplet diameter are consistent with airborne and in-situ measurements[6,7] of similar clouds. The DSD relative dispersion range of $\epsilon \equiv \sigma/r$ of 0.25 and 0.31 on the left and right, respectively, are also broadly consistent with in-situ (flight) measurements, reported in[9,10].

Repeating the procedure along the glory oval, one transect at a time, gives an estimate for the horizontally induced spread of droplet sizes, thus opening a window on separating horizontal and vertical contributions to DSD broadening. Higher satellite resolution (smaller pixel size) is likely to help in such separation as long as the sample volume captures a representative DSD. To the extent that glory structure, along a transect, reflects the DSD optical properties, the more homogeneous the DSD is along the
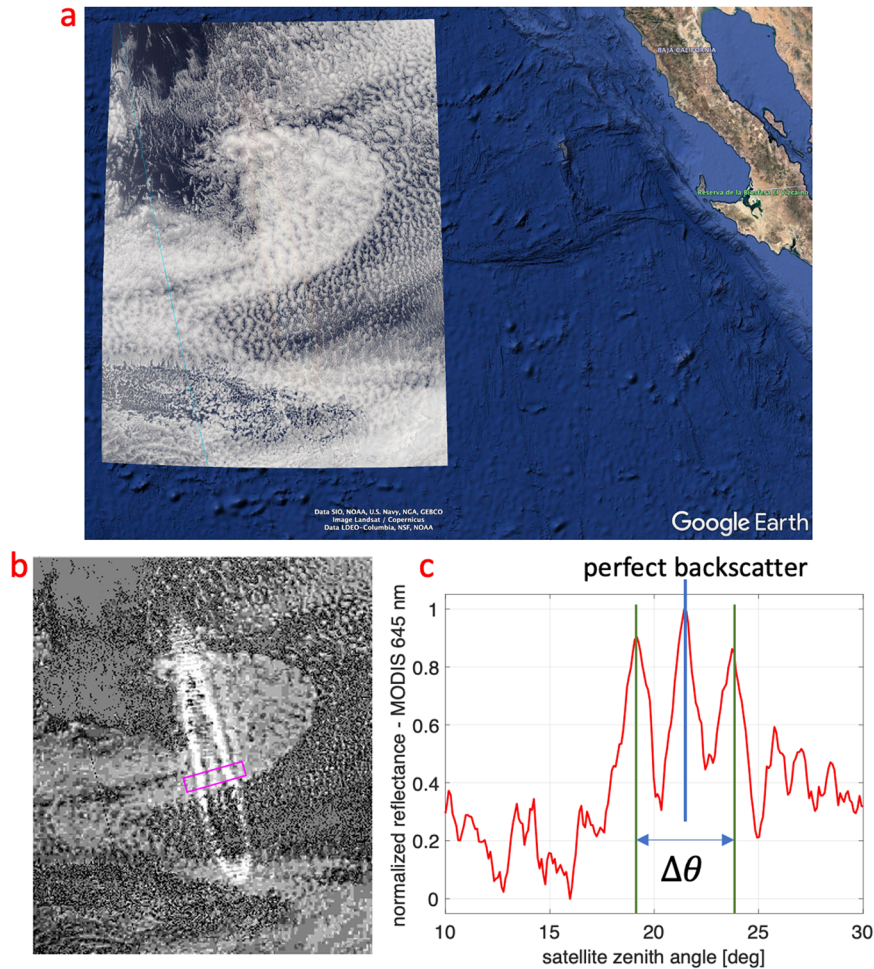
Fig. 2   A faint yet discernible glory in a satellite image of marine Sc west of Baja, CA, taken on May 29, 2021,~13:30 local time, by a moderate resolution imaging spectroradiometer (MODIS) on board the Aqua satellite. a True color image, projected on the Google Earth platform, where a faint glory is discernible near the center and the blue line is the nadir track of Aqua. b Subtracting the red from the blue channel amplifies the glory. Clouds are white because their red and blue reflectances are similar but the difference image captures wavelength-dependent features such as the glory. For the lower part of the glory, despite the clouds there being optically thin, single scattering, causing the glory, displays the first ring, the central backscatter, and a weaker second red ring. The shape of the glory ring permits a geometric estimate of droplet sizes that is tolerant of imperfections in the instrument's calibration and is apparent even for the thinnest clouds. Moreover, the elongation induced by the satellites motion, allows for a broader usage of glory information that could be used to invert droplet properties over wider portion of the cloud field. c Reflectance measured by the MODIS red channel (filter range: 620–670 nm) across the glory as demarcated by the magenta box in b. The glory's signal is evident on either side of the exact backscatter peak, allowing for angular size and related magnitudes conversion to the droplets average diameter and its variance (see Methods).

glory's transect, the better is the inversion. Less variable cloud decks such as those of Sc, will make clearer and sharper glories. These Sc cloud systems are topped by a strong inversion and form under mild instabilities in the boundary layer below it (manifested as relatively weak updrafts)[1]. Such conditions typically result in a rather uniform top of the clouds deck, exhibiting fairly constant profiles and aerosol levels (except for ship tracks), thus yielding the needed homogeneity.

In principle, parts of the glory signal could be seen in broken clouds if the needed homogeneity conditions are met locally for a sufficiently long segment. If so, $\Delta\theta$ could be estimated locally for a warm (liquid water droplets at the top) cloud fragments, detached from the deck. However, the convective clouds, more developed vertically, fluctuate more in top height and have less homogeneous DSDs. Small clouds detached from the deck, or holes in the decks will, likely, contribute to the noise without altering inversion results, except when blocking key features such as the red ring or the exact backscatter.

Since glory is a feature of electromagnetic scattering by spherical particles, it will not form for clouds composed of ice particles (that are aspherical), even if the cloud tops are homogeneous (e.g., clouds anvils). This suggests a lower limit on the cloud's top temperature (possibly containing spherical super-cooled water droplets). Thus, polar stratiform clouds are not likely to create glories. However, because of the required geometric alignment, for the current polar-orbiting satellites, glories can form only within the tropical-subtropical belt. Over these areas, the shallow stratiform clouds are usually warm marine Sc.

Although coronas and glories have been studied for centuries[4,11,12], carefully and extensively simulated[13] as well as compared with aircraft observations recently to invert for droplet size distribution parameters[7], the globe-wide availability of glories on the daily basis and a simple application to satellite imaging via the associated simple diffraction scaling, to the best of our knowledge, has gone undetected. It is remarkable that, unlike rainbows, the index of refraction, seemingly so essential to the Mie scattering

problem, affects the magnitude but not angular pattern of glories, allowing the simple diffraction-like scaling to emerge.

In summary, we presented a "proof of concept" for detecting glories and inverting their properties to extract the much-needed first two moments of the DSD. To that end, we employed the simplest unencumbered version of the method, using solely the red channel. For an operational inversion, other satellite wavelengths will be used to improve robustness of the inversion. Insofar as inverting the glory pattern (Fig. 2c) for the first two moments of DSD, relies on accurate positioning of the peaks and quantifying the amplitude modulation, higher spatial satellite resolution and larger dynamic range will supply a crisper description of the glory structure (ring diameters and intensities). Here we used the MODIS 500 m resolution which allowed for inversion better than 0.1 μm. As shown in Fig. 1a, the projected order onto the horizontal line is always as follows: solar nadir, ocean glint, satellite nadir track, and finally glory. Once a reliable automated detection of glories (an ongoing effort by us) becomes available, the huge, $\sim O(10^4)$, and up-to-now untapped reservoir of information will deliver a statistically exact ($1/\sqrt{N} \sim 10^{-2}$ uncertainty reduction) ensemble droplet size and stringent bounds on the breadth of the size distribution for the vast oceanic sheets of marine Sc, of great importance to the Earth radiative balance[14,15].

METHODS

Glory signal for droplet size distribution

The glory signal for a droplet size distribution is calculated as a superposition of monodisperse contributions of each size bin, weighted by the bin's abundance. Therefore, distribution of droplet sizes causes the ring pattern to blur. In particular, the first ring glory amplitude (GA), relative to the amplitude of the perfect back-scatter (BSA) is diminished. Mie scattering calculations[16] associate each pair of droplet's average radius and variance to a unique pair of glory's ring size and BSA to GA ratio. We used Mie scattering calculations of the glory for a wide range of DSDs and built a lookup table that matches each pair of ($\Delta\theta$,BSA/GA) to a pair (r,σ) of droplet's mean radius ($r \equiv d/2$) and DSD standard deviation.

Satellite zenith angle as a direct measure for glory

The continuously available MODIS satellite zenith angle (SatZA), maps the angular position of each pixel on the surface, relative to one directly below the satellite's orbit (zenith). As shown in Fig. 1a, the location of the glory's projection on the cloud top depends on the sun-satellite-clouds geometry. The extension of the straight line between the sun and the satellite toward the clouds marks the glory's center (exact backscatter) and the glory's angular size is measured by SatZA around it. Figure 2c shows the measured reflectance of the red channel with the MODIS red filter allowing the range of 620 to 670 nm. The reflectance curve is along the middle part of the glory within the magenta box of Fig. 2b, in SatZA units (in degrees). The corresponding SatZA of the exact backscatter data is the angle of the glory projection, denoted as α in Fig. 1a. In this case α = 21.44 ± 0.1° and the glory's width is scaled by cos α, when projected onto the plane, normal to the sun-satellite line (H in Fig. 1a).

Uncertainty estimates

The angular size of the glory's red ring, calculated as the distance between the first two peaks on either side of the exact backscatter (between the two green lines in Fig. 2c) equals $\Delta\theta$ = 4.6 ± 0.14°. The uncertainty in the measurements of angle comes from the pixel size, resulting here in 500 m spatial resolution. The best MODIS resolution of the red channel is 250 m (at nadir) which reduces the uncertainty. However, the uncertainty of the retrieved droplet size caused by these uncertainties is exceeded by the estimated droplet variance. We note the reassuring symmetry of

this glory data: $\Delta\theta$ is partitioned evenly around the exact backscatter point (2.3 ± 0.1° on the left and 2.3 ± 0.1° on the right).

Droplet radius and variance estimates

The amplitude ratio of the perfect backscatter BSA and the glory GA (relative to the minima between them) is BSA/GA = 1.15 and 1.3 on the left and right parts. Using Mie scattering simulations of glories for a wide range of droplets DSD, for each mean radius and a given variance we calculated both $\Delta\theta$ and BSA/GA. The calculations show that each ($\Delta\theta$,BSA/GA) pair is coupled uniquely to the first two DSD's moments (r mean radius and σ standard deviation). The pair ($\Delta\theta$ = 4.6°,BSA/GA = 1.15) corresponds to (r = 6.9 μm, σ = 1.75 μm) and the pair ($\Delta\theta$ = 4.6°,BSA/GA = 1.30) corresponds to (r = 6.6 μm, σ = 2.21 μm).

REFERENCES

1. Feingold, G., Cotton, W. R., Kreidenweis, S. M. & Davis, J. T. The impact of giant cloud condensation nuclei on drizzle formation in stratocumulus: Implications for cloud radiative properties. *J. Atmos. Sci.* **56**, 4100–4117 (1999).
2. Seinfeld, J. & Pandis, S. *Atmospheric Chemistry and Physics. 1997* (New York, 2008).
3. Diamond, M. S. et al. Opinion: To assess marine cloud brightening's technical feasibility, we need to know what to study—and when to stop. *Proc. Natl Acad. Sci. USA* **119**, e2118379119 (2022).
4. Nussenzveig, H. M. The science of the glory. *Sci. Am.* **306**, 68–73 (2012).
5. Israelevich, P., Joseph, J., Levin, Z. & Yair, Y. First observation of glory from space. *Bull. Am. Meteorol. Soc.* **90**, 1772–1774 (2009).
6. Mayer, B., Schröder, M., Preusker, R. & Schüller, L. Remote sensing of water cloud droplet size distributions using the backscatter glory: a case study. *Atmos. Chem. Phys.* **4**, 1255–1263 (2004).
7. Konwar, M., Laven, P. & Prabha, T. Simultaneous observation of a glory and in-situ microphysical cloud properties. *Appl. Opt.* **56**, 5–8 (2017).
8. Nakajima, T. & King, M. D. Determination of the optical thickness and effective particle radius of clouds from reflected solar radiation measurements. part i: Theory. *J. Atmos. Sci.* **47**, 1878–1893 (1990).
9. Wang, Y. et al. Dispersion of droplet size distributions in supercooled non-precipitating stratocumulus from aircraft observations obtained during the southern ocean cloud radiation aerosol transport experimental study. *J. Geophys. Res.: Atmos.* **126**, 2020–033720 (2021).
10. Jia, H., Ma, X. & Liu, Y. Exploring aerosol–cloud interaction using vocalsrex aircraft measurements. *Atmos. Chem. Phys.* **19**, 7955–7971 (2019).
11. Van de Hulst, H. A theory of the anti-coronae. *JOSA* **37**, 16–22 (1947).
12. Ramachandran, G. The theory of coronae and of iridescent clouds. *Proc. Indian Acad. Sci.-Section A* **17**, 202–218 (1943).
13. Laven, P. Atmospheric glories: simulations and observations. *Appl. Opt.* **44**, 5667–5674 (2005).
14. Twomey, S. The influence of pollution on the shortwave albedo of clouds. *J. Atmos. Sci.* **34**, 1149–1152 (1977).
15. Twomey, S. Pollution and the planetary albedo. *Atmos. Environ.* **8**, 1251–1256 (1974). (1967).
16. Bohren, C. F. & Huffman, D. R. *Absorption and Scattering of Light by Small Particles* (John Wiley & Sons, New Jersey, 2008).

AUTHOR CONTRIBUTIONS

I.K. and A.K. conceived the idea, developed the theoretical concept and wrote the paper. U.W. and D.D. contributed substantially to all aspects of simulations, data analysis and interpretation of the results.

COMPETING INTERESTS

The authors declare no competing interests.

ADDITIONAL INFORMATION

Correspondence and requests for materials should be addressed to Ilan Koren.

Reprints and permission information is available at http://www.nature.com/reprints